References

ALLEN, F. H., BELLARD, S., BRICE, M. D., CARTWRIGHT, B. A., DOUBLEDAY, A., HIGGS, H., HUMMELINK, T., HUMMELINK-PETERS, B. G., KENNARD, O., MOTHERWELL, W. D. S., RODGERS, J. R. & WATSON, D. G. (1979). *Acta Cryst.* B**35**, 2331–2339.

ANDERSEN, A. M. (1975*a*). *Acta Chem. Scand. Ser. B*, **29**, 239–244.

ANDERSEN, A. M. (1975*b*). *Acta Chem. Scand. Ser. B*, **29**, 871–876.

ANDERSEN, A. M. (1977). *Acta Chem. Scand. Ser. B*, **31**, 162–166.

ANDERSEN, A. M., MOSTAD, A. & RØMMING, C. (1972). *Acta Chem. Scand.* **26**, 2670–2680.

ARMSTRONG, J. & BARLOW, R. B. (1976). *Br. J. Pharmacol.* **57**, 501–516.

BARLOW, R. B. (1987). Unpublished measurements.

BARLOW, R. B., BOWMAN, F., ISON, R. R. & MCQUEEN, D. S. (1974). *Br. J. Pharmacol.* **51**, 585–597.

BARLOW, R. B. & GONZÁLEZ, J. L. (1986). *Arch. Farmacol. Toxicol.* **12**, 87–98.

BARLOW, R. B. & HAMILTON, J. T. (1962). *Br. J. Pharmacol. Chemother.* **18**, 543–549.

BARLOW, R. B. & HAMILTON, J. T. (1965). *Br. J. Pharmacol. Chemother.* **25**, 206–212.

BARLOW, R. B., HOWARD, J. A. K. & JOHNSON, O. (1986). *Acta Cryst.* C**42**, 853–856.

BARLOW, R. B. & JOHNSON, O. (1988). Unpublished measurements.

BARLOW, R. B. & MCLEOD, L. J. (1969). *Br. J. Pharmacol.* **35**, 161–174.

BARLOW, R. B., THOMPSON, G. M. & SCOTT, N. C. (1969). *Br. J. Pharmacol.* **37**, 555–584.

BERGIN, R. (1971). *Acta Cryst.* B**27**, 2139–2146.

BERGIN, R. & CARLSTROM, D. (1968). *Acta Cryst.* B**24**, 1506–1510.

BEURSKENS, P. T., BOSMAN, W. P., DOESBURG, H. M., GOULD, R. O., VAN DEN HARK, TH. E. M., PRICK, P. A. J., NOORDIK, J. H., BEURSKENS, G., PARTHASARATHI, V., BRUINS-SLOT, H. J., HALTIWANGER, R. C., STRUMPEL, M. & SMITS, J. M. M. (1984). *DIRDIF* system. Tech. Rep. 1984/1. Crystallography Laboratory, Toernooiveld, 6525 ED Nijmegen, The Netherlands.

CARLSTROM, D. & BERGIN, R. (1967). *Acta Cryst.* **23**, 313–319.

DALE, H. H. & LAIDLAW, P. P. (1912). *J. Pharmacol. Exp. Ther.* **3**, 205–221.

GIESECKE, J. (1980). *Acta Cryst.* B**36**, 178–181.

HAMOR, T. A. & JONES, R. H. (1982). *Acta Cryst.* B**38**, 1007–1009.

International Tables for X-ray Crystallography (1974). Vol. IV. Birmingham: Kynoch Press. (Present distributor Kluwer Academic Publishers, Dordrecht.)

MATHEW, M. & PALENIK, G. J. (1971). *J. Am. Chem. Soc.* **93**, 497–502.

MURRAY-RUST, P. & MOTHERWELL, W. D. S. (1978). *Acta Cryst.* B**34**, 2518–2526.

PODDER, A., DATTAGUPTA, J. K., SACHA, N. N. & SAENGER, W. (1979). *Acta Cryst.* B**35**, 649–652.

SHELDRICK, G. M. (1981). *SHELXTL. An Integrated System for Solving, Refining and Displaying Crystal Structures from Diffraction Data.* Univ. of Göttingen, Federal Republic of Germany.

SHELDRICK, G. M. (1988). *SHELXTL-Plus.* Software package for the Nicolet *R3m/V* and *R3m/V*2000 Crystallographic Research Systems. Nicolet Instrument Corporation, Madison, Wisconsin, USA.

TAMURA, K., WAKAHARA, A., FUJIWARA, T. & TOMITA, K.-I. (1974). *Bull. Chem. Soc. Jpn*, **47**, 2682–2685.

TSOUCARIS, G. (1961). *Acta Cryst.* **14**, 909–917.

TSOUCARIS, D., DE RANGO, C., TSOUCARIS, G., ZELWER, C., PARTHASARATHY, R. & COLE, F. E. (1973). *Cryst. Struct. Commun.* **2**, 193–196.

Acta Cryst. (1989). B**45**, 404–411

Structural Phase Transition in 1-Chloroadamantane ($C_{10}H_{15}Cl$)

BY M. FOULON, T. BELGRAND, C. GORS AND M. MORE

Laboratoire de Dynamique des Cristaux Moléculaires (UA 801 CNRS), UFR de Physique Fondamentale, Batiment P5, Université des Sciences et Techniques de Lille I, 59655 *Villeneuve d'Ascq CEDEX, France*

(*Received* 20 *September* 1988; *accepted* 27 *February* 1989)

Abstract

The structures of the high-temperature plastic disordered (I) and low-temperature ordered (III) phases of 1-chloroadamantane ($C_{10}H_{15}Cl$, $M_r = 170{\cdot}5$, symmetry C_{3v}) were investigated by X-ray diffraction analysis [$\lambda(\text{Mo } K\bar{\alpha}) = 0{\cdot}7107$ Å, $\mu = 0{\cdot}27$ cm^{-1}, $F(000) = 157$]. Phase I crystallizes in the cubic space group $Fm3m$ and was studied at two temperatures [$a = 9{\cdot}970$ (10) Å at 295 K and $9{\cdot}864$ (10) Å at 257 K, $Z = 4$, $D_x(295\text{ K}) = 1{\cdot}14$ g cm^{-3}, D_m not measured]. The structural analysis confirms the assumptions made in interpreting the dynamical disorder observed by NMR, IQNS and dielectric relaxation measurements. The molecule undergoes a tumbling movement of its C_3 axis between the fourfold crystallographic axes, and a fast uniaxial rotation about the C_3 molecular axis. Steric hindrance analysis showed that ferro- or antiferroelectric local configurations are favoured. Phase III crystallizes in the monoclinic space group $P2_1/c$ [$a = 10{\cdot}018$ (10), $b = 6{\cdot}823$ (7), $c = 13{\cdot}147$ (13) Å, $\beta = 90{\cdot}04$ (4)°, $V = 898{\cdot}7$ Å^3, $Z = 4$, $D_x = 1{\cdot}26$ g cm^{-3}, D_m not measured, $T = 210$ K, $R = 0{\cdot}034$ for 1036 observed reflections]. The procedure for obtaining and selecting good crystals at $T < T_t$ (T_t = transition temperature) is briefly described. In phase III, the molecule takes only one equilibrium position in a lattice site. The threefold axis is fixed and

0108-7681/89/040404-08$03.00

the tumbling movement is frozen. The dynamical molecular movement detected by NMR experiments must then be interpreted as a uniaxial threefold rotation about the C_3 molecular axis. The molecular axes lie in planes $x/a = \frac{1}{4}$ and $\frac{3}{4}$, perpendicular to one another in the same plane. The transition mechanism is best understood by constructing a pseudo-cubic lattice on the basis of the monoclinic lattice vectors. From this, it is clear that the transition is destructive as six domains are created when going from the high- to the low-temperature phase.

1. Introduction

This work is part of a series of studies on the properties of adamantane ($C_{10}H_{16}$, ADM hereafter) and its 1-monosubstituted derivatives (1-*X*-ADM, X = F, Cl, Br, CN or I) (Foulon, 1987). These compounds are obtained by hydrogen substitution on a tertiary carbon of ADM. This causes lowering of the molecular symmetry from T_d (ADM) to C_{3v} (1-*X*-ADM) and creation of an axial dipole moment along the C_3 axis (3·92 debye for 1-CN-ADM and 2·39 debye for 1-Cl-ADM, 1 debye = $3{\cdot}336 \times 10^{-30}$ C m).

1-Cl-ADM (Fig. 1), like other derivatives (Chang & Westrum, 1960; Amoureux & Bee, 1979; Foulon, Lefebvre, Amoureux, Muller & Magnier, 1985), presents an orientationally disordered phase, the so-called plastic phase (phase I). A thermodynamical study of phase transitions made by differential scanning calorimetry confirmed previous experiments (Clark, McKnox, Mackle & McKervey, 1977). Our measurements show that the solid–solid transition occurs at 246 K. By analogy with 1-Br-ADM, which exhibits two (ordered and semi-ordered) phases below phase I, the low-temperature phase of 1-Cl-ADM was indexed as phase III (Fig. 2). At the first-order transition from phase III to phase I, the enthalpy is greater than that of melting. This is characteristic of such transitions and indicates the appearance of significant disorder. In contrast to 1-CN-ADM (Foulon, Lefebvre, Amoureux, Muller & Magnier, 1985; Foulon, Amoureux, Sauvajol, Cavrot & Muller, 1984), the quenching of 1-Cl-ADM down to 100 K does not reveal any 'glassy crystal' phase.

A previous structural study of the plastic phase of 1-Cl-ADM (Amoureux, Bee & Sauvajol, 1982) showed the following features:

(*a*) A face-centred cubic lattice with space group *Fm*3*m*.

(*b*) The centres of mass of the adamantyl groups are distributed among the lattice sites.

(*c*) In one site, a molecule can take at least 24 equilibrium positions. The threefold molecular axis is equiprobably oriented along any one of the six fourfold lattice directions. In each orientation, the molecule can occupy four equilibrium positions related by $\pi/6$ rotations around the molecular axis.

Because of the relatively high values of the reliability factors, this study may be improved, particularly the molecular thermal-motion description. NMR, IQNS and dielectric relaxation studies (Amoureux, 1980; Bee & Amoureux, 1983; Ursu, Grosescu, Lupu & Lazarescu, 1983; Virlet, Quiroga, Boucher, Amoureux & Castelain, 1983) have revealed that in phase I, molecules reorientate rapidly from one fourfold cubic axis to another (tumbling) and rotate about the molecular threefold axis (uniaxial rotation) (Table 1). This dynamical disorder is accompanied by a strong translational diffusion (Ursu, Grosescu, Lupu & Lazarescu, 1983). The transition to the low-temperature phase corresponds to freezing of the tumbling movement. The uniaxial rotation still remains but is much slower than in phase I.

Our aim was to obtain more accurate information about the plastic phase and to determine the structure of the low-temperature phase; from this we expected to gain a better understanding of the transition mechanism between the two phases.

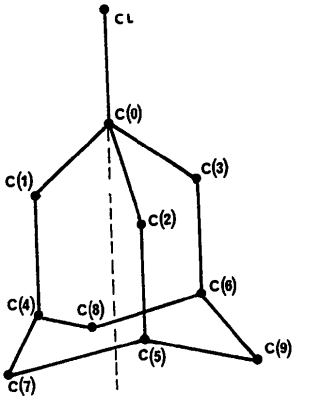

Fig. 1. Atom numbering of the 1-chloroadamantane molecule.

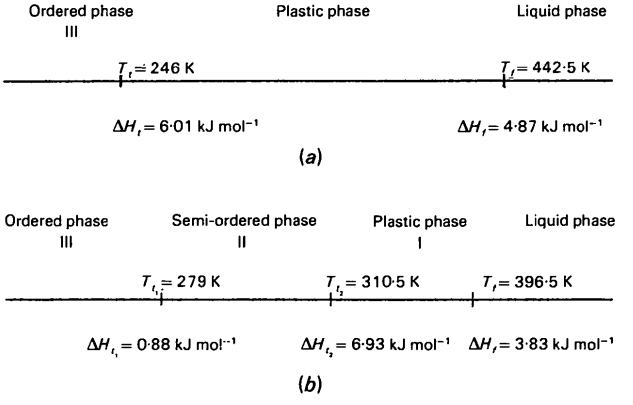

Fig. 2. Phase-transition sequence in (*a*) 1-chloro- and (*b*) 1-bromo-adamantane (Clark *et al.*, 1977).

Table 1. *Residence times of the different molecular movements in* 1-*chloroadamantane*

τ_{C_3} is for the tumbling movement about threefold cubic lattice axes. τ_{Mp} is for the uniaxial rotation motion of order p about threefold molecular axis. $\tau = \tau_0 \exp(E/T)$ (Amoureux, 1980).

		τ_0(× 10^{14}) (s)	E (kJ mol^{-1})	At the melting point (442·5 K)	At the transition temperature (244·2 K)
Phase I	τ_{C_3}	1·09	10·28	$1{\cdot}8 \times 10^{-13}$ s	$1{\cdot}7 \times 10^{-12}$ s
	τ_{M12}	1·23	21·41	$4{\cdot}1 \times 10^{-12}$ s	$4{\cdot}7 \times 10^{-10}$ s
Phase III	τ_{M3}	—	—	—	—

Table 2. *Data-collection parameters for the high- and low-temperature phases*

N is the total number of collected data, N_{ne} is the number of nonequivalent reflections, N_t is the number of reflections with $F_{obs} > 3\sigma$ for the high-temperature plastic phase and $F_{obs} > 6\sigma$ for the low-temperature phase.

	T (K)	θ range (°)	Scan speed (° s^{-1})	Scan width (°)	N N_{ne}	N_t	h,k,l range
Phase I	295	0–30	0·01	1·2	121 103	34	
	257	0–31	0·02	1·2	305 110	45	
Phase III	210	0–25	0·04	1·2	1652 1343	1036	$-11 < h < 11$ $0 < k < 7$ $0 < l < 14$

As a result of the destructive nature of the I⟷III transition, we had to carry out crystallization and selection of the samples at low-temperature ($T <$ 230 K). The purification of the product was performed by sublimation and recrystallization. Gas chromatography and NMR were used to test the degree of purity.

2. Experimental

2.1. *Samples*

For the plastic phase, bipyramidal crystals were grown by slow evaporation of a solution in methanol at room temperature. This volatile compound has a sticky texture and must be introduced into a Lindemann capillary.

Crystal growth of the low-temperature phase was performed by slow cooling of a solution of 1-Cl-ADM in methanol previously saturated at 235 K. Crystals are parallelepipedic and translucent. To choose a good crystal for the X-ray investigations, samples were transferred to an isothermal box at 223±2 K (Fig. 3*a*). Nitrogen or methanol circulation maintained the low temperature, temperature regulation being carried out using a cryostat (Haake KT60). Since there is no efficient glue at such temperatures, the sample (volume 0·017 mm^3) was introduced into a Lindemann capillary and mechanically blocked using a glass rod. Transfer of the sample from the isothermal box to the diffractometer was realized by covering the capillary with a brass cylinder and placing it in a Dewar vessel filled with dry ice (Fig. 3*b*).

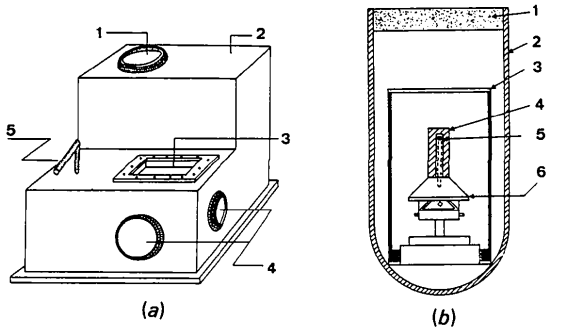

Fig. 3. (*a*) Isothermal box for growth and selection of the crystals: 1, air-tight gate; 2, fluid exit; 3, window; 4, hand passage; 5, fluid entry. (*b*) Crystal protection for transfer to the diffractometer: 1, isolating cover; 2, dewar vessel; 3, plexiglass holder; 4, brass cylinder; 5, crystal; 6, goniometer head.

2.2. *X-ray investigations*

Philips PW1100 diffractometer. 25 reflections used for measuring lattice parameters. θ–2θ scan mode. Monochromatized Mo $K\bar{\alpha}$ radiation. No absorption correction applied ($\mu = 0{\cdot}27$ cm^{-1}). Intensities corrected for LP factor. The data-collection parameters, together with the number of reflections recorded, are given in Table 2.*

2.2.1. *Plastic phase.* Studies at 295 and 257 K, three standard reflections $\langle\sigma(I)/I\rangle = 0{\cdot}01$. The crystals showed very low mosaicity [full-width at half maximum (FWHM) of reflection (311) was 0·12°].

2.2.2. *Low-temperature phase.* Studies at 185 and 210 K. The 185 K study was interrupted by a technical problem and the results were only used for lattice-parameter determination. At 210 K, three standard reflections $\langle\sigma(I)/I\rangle = 4 \times 10^{-3}$. The sample was of good quality with FWHM < 0·15°.

3. Structure refinements

3.1. *Plastic phase at* 295 *and* 257 K

Three models can be used to describe such a disordered structure:

(*a*) The Frenkel model which considers a mean molecule describing N equilibrium positions each with $1/N$ Dirac probability.

* Lists of structure factors and H-atom parameters for phase III at 210 K have been deposited with the British Library Document Supply Centre as Supplementary Publication No. SUP 51724 (9 pp.). Copies may be obtained through The Executive Secretary, International Union of Crystallography, 5 Abbey Square, Chester CH1 2HU, England.

Table 3. *Results of the refinements for plastic phase* I

U_3 is the distance between the adamantyl centre of mass and the lattice origin, N is the number of reflections included in the refinements.

						Without reflections (200) and (111)			With reflections (200) and (111)			All Reflections		
Model	T (K)	U_3 (Å)	$T_{11}^{1/2}$ (Å)	$T_{33}^{1/2}$ (Å)	$L_{11}^{1/2}$ (°)	R (%)	wR (%)	N	R (%)	wR (%)	N	R (%)	wR (%)	N
CED, isotropic	257	−0·046 (9)	0·27 (1)	$= T_{11}^{1/2}$	4·7 (3)	9·4	9·0	31	7·7	8·9	33	10·1	11·8	45
	295	−0·028 (17)	0·33 (2)	$= T_{11}^{1/2}$	5·2 (4)	13·8	11·0	26	11·7	11·1	28	13·1	11·5	34
CED, anisotropic	257	−0·036 (10)	0·24 (2)	0·29 (1)	5·2 (3)	9·8	8·1	31	7·8	8·0	33	10·4	10·9	45
	295	−0·024 (17)	0·30 (3)	0·34 (2)	5·5 (5)	13·8	10·6	26	12·2	10·9	28	13·6	11·3	34
Frenkel*	295	0	0·32 (2)	0·41 (2)	8·1 (3)							9·0	18·1	112
CED*	295	0	0·30 (3)	0·39 (3)	8·6 (4)							—	22·0	112
SAF*	295	0	$T_{11}^{1/2} = T_{22}^{1/2} = T_{33}^{1/2}$ 0·41 (3)		7							—	13·8	112

* Amoureux, Bee & Sauvajol (1982).

(*b*) The SAF model. This involves analysis of the molecular orientational probability by structure-factor decomposition on functions adapted to the site and molecule symmetry (Press & Hüller, 1973; Seymour & Pryor, 1970).

(*c*) The cylindrical electronic density (CED) model (Amoureux, Bee & Sauvajol, 1982; Foulon, Lefebvre, Amoureux, Muller & Magnier, 1985), which allows a description of uniaxial disorder corresponding to a large number of positions around a fixed axis.

Our study confirms that the molecule is in space group $Fm3m$ with $a = 9{\cdot}970\ (10)$ Å at 295 K and 9·864 (10) Å at 257 K. Only reflections for which $F_{obs} > 3\sigma$ were used in the refinements (Table 2), with the following weighting scheme: $w = 1/\sigma^2(F)$ where $\sigma(F) = K(\sigma^2 + E^2F_{obs}{}^2)^{1/2}$ and $K = 48p$, p being the multiplicity of the reflection. Two reflections (200 and 111), which were very strong but weakened by extinction, were omitted in a first stage of the refinements. The thermal motion in phase I led us to omit reflections with $h^2 + k^2 + l^2 > 100$. Combination of the Frenkel and CED models led to a good description of the structure.

The molecular geometry is constructed according to previous studies on the adamantyl group. The C0—Cl bond distance is fixed at the value found in the study of the low-temperature phase determined earlier (for numbering see Fig. 1). An individual molecule is assumed to be a rigid group.

Considering a molecule with a fixed orientation in the lattice (for example, $C_3 \parallel \mathbf{c}$), the disorder was described by the CED model. The different orientations of the molecule in the lattice site are generated by $m3m$ symmetry according to the Frenkel model. Then, only five parameters had to be refined: the scale factor, T_{11}, T_{33}, L_{11} and U_3. U_3 represents the distance between the centre of mass of the adamantyl group and the lattice origin. The mean-square amplitudes, T_{11} ($=T_{22}$) and T_{33}, are the nonvanishing components of the translation **T** tensor. L_{11} ($=L_{22}$) is the single component of the libration **L** tensor: the CED model leads to $L_{33} = 0{\cdot}0$. (The indices 11 denote vibrations perpendicular to the C_3 molecular axis and 33 denote vibrations along this axis.) Refinement of the nonvanishing S_{12} component of the translation–libration coupling tensor **S** leads to a non-significant low value. This S_{12} term was cancelled.

Applying this model to the data of Amoureux (Amoureux, Bee & Sauvajol, 1982) gives the results reported in Table 3. The refinements of our data introducing an isotropic ($T_{11} = T_{33}$) or anisotropic ($T_{11} \neq T_{33}$) **T** tensor, led to more reliable results (Table 3) owing to the better quality crystal. Our study confirms that the molecule takes six orientations along the ⟨001⟩ axes in one site. The success of the CED model proves that the molecule can occupy a great number of positions around its C_3 axis.

The thermal-vibration coefficients are lower than those supplied by Amoureux, particularly the L_{11} term, which is less than half the previous value. These important differences probably occur because high-order reflections were taken into account by Amoureux. Considering our analysis, isotropic or anisotropic descriptions of thermal motion lead to comparable reliability factors. Using the Hamilton test (Hamilton, 1965; Hamilton & Abrahams, 1972), it is shown that the anisotropic model is more reliable than the isotropic one at 257 K. This last model can be rejected with a low probability error ($\alpha = 0{\cdot}025$). However, at 295 K, the isotropic model cannot be rejected ($\alpha = 0{\cdot}25$). When lowering the temperature, the ratio T_{33}/T_{11} increases [1·28 (11) at 295 K and 1·48 (13) at 257 K]. It shows that the molecular translational vibrations become more anisotropic when the transition temperature is approached. In spite of the fast tumbling movement, the L_{11} term, characteristic of libration perpendicular to the C_3 molecular axis, is of low magnitude ($L_{11}^{1/2} = 5{\cdot}2$ at 295 K) (Table 3). The U_3 excentricity parameter is

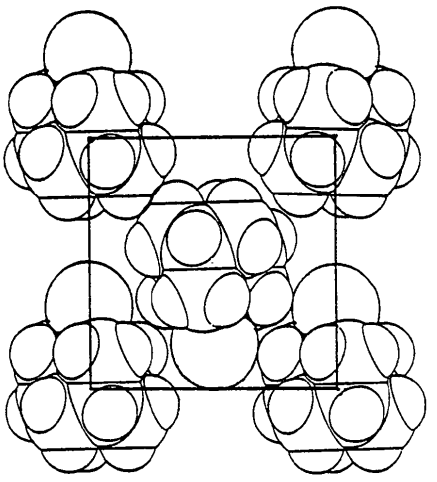

(a)

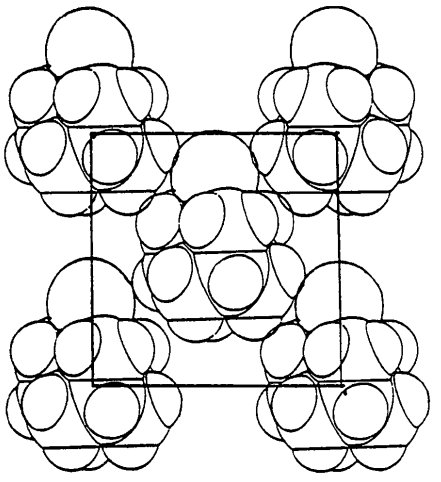

(b)

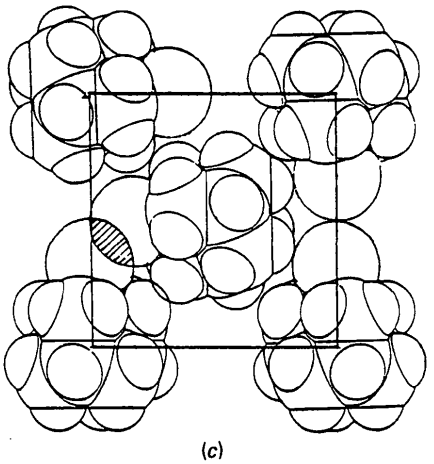

(c)

Fig. 4. Projections of the high-temperature plastic phase structure in the (001) plane, showing different local arrangements: (*a*) antiferroelectric, (*b*) ferroelectric, (*c*) improbable orientation.

Table 4. *Lattice parameters* (Å,°) *of the low-temperature phase at* 185 *and* 210 K

Temperature	*a*	*b*	*c*	*β*	*V* (Å^3)
185 K	10·017 (10)	6·809 (7)	13·141 (13)	90·05 (9)	896 (3)
210 K	10·018 (10)	6·823 (7)	13·148 (13)	90·04 (9)	899 (3)

weak but increases when lowering the temperature. This may be related to anharmonic phenomena.

Projections of the structure along [001] are presented in Figs. 4(*a–c*). They show particular local configurations where the dipolar axes lie in the same plane. The probability of finding nearest neighbouring molecules with their axes perpendicular to one another is low (Fig. 4*c*). However, local arrangements where first- and second-nearest neighbours have their axis parallel or antiparallel are more probable (Figs. 4*a,b*). In a similar compound, 1-Br-ADM, the Kirkwood factor deduced from DR measurements (Virlet, Quiroga, Boucher, Amoureux & Castelain, 1983) predicts an antiferroelectric local order. This can mean that, in such structures and compounds, dipole–dipole interactions are important and govern the mutual orientations of the dipolar axes.

3.2. *Low-temperature phase at* 210 K

3.2.1. *Refinement and molecular arrangement.* At the two experimental temperatures, the cell parameters (Table 4) suggest an orthorhombic lattice but measurements of the intensities for some equivalent reflections showed unambiguously that phase III crystallizes in the monoclinic system $[I(h,k,l) = I(h,\bar{k},l) \neq I(\bar{h},k,l) = I(h,k,\bar{l})]$. The unit cell contains four molecules in general positions with respect to the space group $P2_1/c$. $D_x = 1{\cdot}26$ g cm^{-3} at 210 K (D_m not measured). C atoms were localized by successive direct and difference Fourier maps. 1036 reflections $[I > 3\sigma(I)]$ were used in the refinements with the weighting scheme derived from $\sigma(I)$ $[w = 1/\sigma^2(F)]$. In the first stage of refinement, the atoms were considered independent (*SHELX*, Sheldrick, 1976). At the end of the refinements $\langle \Delta/\sigma \rangle = 0{\cdot}3$. The final difference Fourier map showed no significant residual electronic density ($\rho_{max} = 0{\cdot}2$, $\rho_{min} = -0{\cdot}15$ e Å^{-3}). $R = 0{\cdot}034$ and $wR = 0{\cdot}038$ for 161 refined parameters. The final atomic coordinates and thermal-motion factors of the heavy atoms are reported in Table 5. Intramolecular distances and angles, uncorrected for libration effects lead to a molecular geometry in agreement with C_{3v} molecular symmetry and T_d of the pseudo-adamantane group. The C0—Cl bond is longer [1·827 (3) Å] than that generally encountered (1·77 Å). Such deviations from the standard value have already been reported in similar molecules (Hovmoller, Smith & Kennard, 1978; Shields & Kennard, 1983).

In a second stage, we performed rigid-group refinements using the *ORION* program (André, Fourme &

Table 5. *Atomic coordinates* ($\times 10^4$) *and thermal agitation tensors* ($Å^2 \times 10^4$) *of the low-temperature phase at* 210 K

$$U_{ij} = (2\pi^2 a_i^* a_j^*)^{-1}(h^2 a_i^{*2} + \cdots + 2hka_i^* a_j^* + \cdots).$$

	x	y	z	U_{11}	U_{22}	U_{33}	U_{23}	U_{13}	U_{12}
Cl	2718 (1)	6266 (1)	3050 (1)	627 (5)	607 (5)	417 (4)	−145 (3)	8 (3)	47 (4)
C0	2610 (2)	4515 (4)	2001 (2)	389 (13)	336 (13)	302 (12)	−18 (10)	20 (10)	44 (10)
C1	1145 (2)	4036 (4)	1814 (2)	309 (13)	443 (16)	441 (14)	67 (13)	56 (11)	74 (12)
C2	3224 (3)	5449 (4)	1057 (2)	385 (14)	298 (13)	411 (13)	28 (11)	40 (11)	18 (11)
C3	3378 (3)	2663 (4)	2274 (2)	386 (14)	473 (16)	401 (14)	126 (13)	2 (12)	79 (13)
C4	1051 (2)	2598 (4)	933 (2)	270 (13)	419 (15)	587 (16)	−16 (13)	−20 (12)	−14 (11)
C5	3123 (2)	4003 (4)	173 (2)	378 (13)	367 (13)	342 (12)	61 (11)	62 (10)	54 (11)
C6	3279 (3)	1231 (4)	1386 (2)	398 (14)	300 (14)	588 (16)	111 (13)	−12 (12)	130 (11)
C7	1658 (3)	3516 (4)	−22 (2)	417 (14)	427 (16)	396 (14)	−11 (13)	−53 (11)	121 (12)
C8	1816 (3)	729 (4)	1192 (3)	461 (15)	346 (15)	644 (19)	38 (14)	38 (14)	−60 (12)
C9	3884 (3)	2138 (4)	436 (2)	333 (14)	386 (15)	489 (16)	−50 (13)	20 (12)	67 (11)

Table 6. *Thermal-motion analysis of the low-temperature phase at* 210 K *by* **T, L, S** *tensors*

ij components	11	22	33	12	13	23	21	31	32
L (deg²)*									
from U_{ij}	16·28 (96)	14·27 (145)	18·40 (154)	−3·74 (92)	−1·96 (94)	4·60 (103)	$=L_{12}$	$=L_{13}$	$=L_{23}$
from rigid group	16·61 (82)	15·46 (121)	21·50 (131)	−3·58 (66)	−1·25 (79)	4·27 (72)	$=L_{12}$	$=L_{13}$	$=L_{23}$
T (Å²)									
from U_{ij}	0·0302 (10)	0·0304 (9)	0·0349 (9)	0·0041 (8)	0·0010 (8)	0·0049 (7)	$=T_{12}$	$=T_{13}$	$=T_{23}$
from rigid group	0·0270 (11)	0·0307 (5)	0·0374 (9)	0·0030 (5)	0·0009 (5)	0·0045 (5)	$=T_{12}$	$=T_{13}$	$=T_{23}$
S (Å rad)									
from U_{ij}	0·0003 (5)	0·0003 (3)	−0·0006 (22)	−0·0033 (3)	−0·0016 (3)	0·0010 (3)	0·0018 (3)	−0·0014 (4)	−0·0001 (4)
from rigid group	$S_{11}-S_{22}$	$S_{22}-S_{33}$	$S_{33}-S_{11}$						
	0·0001 (4)	0·0004 (6)	−0·0005 (10)	−0·0029 (3)	−0·0016 (3)	0·0009 (3)	0·0015 (3)	−0·0012 (4)	0·0000 (4)

Renaud, 1971). The molecule was placed in the previously determined position. The thermal vibrations are now described by the 20 general coefficients of the **T, L** and **S** tensors (Schomaker & Trueblood, 1968). In this thermal analysis the molecular centre of mass is taken as the origin. The refinements of (**u**, θ) describing the molecular position and orientation in the cell, confirm the results obtained by the independent-atom method and lead to the following reliability factors: $R = 0{\cdot}045$, $wR = 0{\cdot}031$.

Fig. 5 shows a projection of the structure along the **a** axis. The molecular centres of mass and the dipolar axes lie nearly in planes $x/a = \frac{1}{4}$ (m_1) and $\frac{3}{4}$ (m_2) respectively for molecules denoted 1,2 and 3,4. One of the molecular symmetry planes defined by the Cl, C0, C1, C4 and C9 atoms is always nearly perpendicular to the m_1 and m_2 planes. The C1—C4 bond is nearly parallel to these planes, under m_1 for molecules 1 and 2, and above m_1 for molecules 3 and 4. The threefold molecular axes are slightly tilted out of these planes (Fig. 6). Molecular planes m_1 and m_2 do not belong to space group $P2_1/c$, and hence the molecule can only take one distinct position in one site.

3.2.2. *Thermal vibrations – comparison with the plastic phase.* Table 6 shows the elements of the **T, L** and **S** tensors obtained by direct rigid-group refinement and those derived from the U_{ij} parameters (Schomaker & Trueblood, 1968). The agreement between the results confirms that the 1-Cl-ADM molecule may be considered as a rigid group.

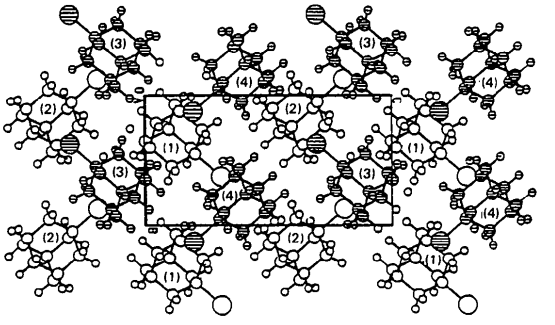

Fig. 5. Projection of the low-temperature phase structure along the monoclinic **a** axis. Molecules (1) and (2) are in planes $x/a = \frac{1}{4}$ (○) and molecules (3) and (4) are in planes $x/a = \frac{3}{4}$ (⊜).

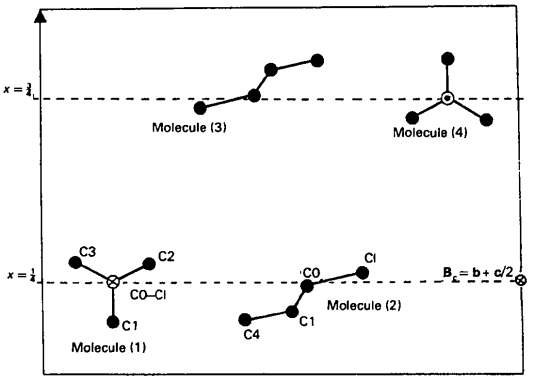

Fig. 6. Representation of the tilting of the molecular axis out of the planes $x/a = \frac{1}{4}$ and $\frac{3}{4}$.

The comparison between the thermal-vibration coefficients of phases I and III leads to the following conclusions about the disorder:

(*a*) In phase I, the L_{11} term is of the same magnitude as the eigen values of the libration amplitudes in the ordered phase III. This means that L_{11} transmits only a 'pure' libration, like L_{ii} in the ordered phase. The fast tumbling movement in the plastic phase then has no significant influence on the librational amplitude perpendicular to the C_3 molecular axis.

(*b*) In the plastic phase, the mean-square translational amplitudes are much larger than in the ordered phase and mainly take the disorder into account.

(*c*) In phase III, no eigen librational vectors lie along the molecular axis, in spite of the uniaxial rotation motion of the molecule (Amoureux, 1980). Therefore, the **L** tensor does not transmit this slow molecular motion.

(*d*) In phase III, the libration–translation coupling tensor coefficients **S** are weak.

4. Structural relations between phases I and III

In the ordered phase III, the centres of mass of the adamantyl group describe a pseudo-f.c.c. lattice defined by the $\mathbf{A}_c$, $\mathbf{B}_c$, $\mathbf{C}_c$ vectors. These are related to the monoclinic vectors (**a**, **b**, **c**) by the following transformations:

$$\mathbf{A}_c = \mathbf{a}; \quad \mathbf{B}_c = \mathbf{b} + \mathbf{c}/2; \quad \mathbf{c}_c = -\mathbf{b} + \mathbf{c}/2.$$

At 210 K, the calculated parameters are:

$$|\mathbf{A}_c| = 10{\cdot}018 \text{ Å}; \quad |\mathbf{B}_c| = |\mathbf{C}_c| = 9{\cdot}974 \text{ Å};$$

$$\angle(\mathbf{B}_c,\mathbf{C}_c) = 92{\cdot}1°.$$

At the phase transition, the cell volume decreases discontinuously ($\Delta V/V = 6\%$; Fig. 7). This explains the destructive nature of the transition.

The structural description of the low-temperature phase, using the pseudo-f.c.c. lattice, points out that the transition I→III leads to an important contraction of the ($\mathbf{B}_c$, $\mathbf{C}_c$) plane ($\Delta\mathbf{B}_c/\mathbf{B}_c = 4\%$) and a weaker dilation along the $\mathbf{A}_c$ axis (1·6%).

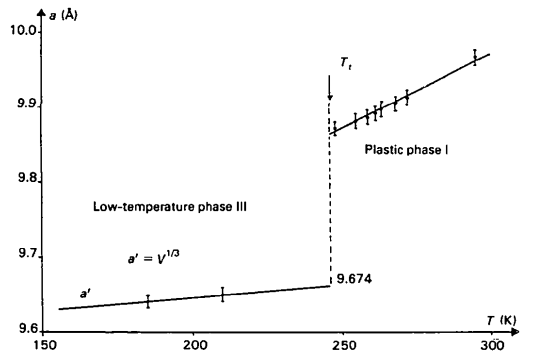

Fig. 7. Evolution of $V^{1/3}$ (where V is the cell volume) in phases I and III.

At the phase transition, the centres of mass of the adamantyl groups undergo important translations (0·3 to 0·65 Å) along the cubic lattice directions ⟨001⟩, ⟨011⟩, ⟨0$\bar{1}$1⟩, ⟨111⟩, ⟨$\bar{1}$20⟩. In the low-temperature phase, the dipolar axes are nearly parallel to the pseudo-fourfold axes and orthogonal to each other in planes $x/A_c = \frac{1}{4}$ and $x/A_c = \frac{3}{4}$ (Fig. 8*a*). In one site, the molecule is locked in a single orientation. There are four distinct orientations in the cell. Fig. 8(*b*) shows a projection along the A_c axis of the four different orientations relative to the pseudo-cubic lattice. It is clearly seen (Fig. 8*a*), that this pseudo-f.c.c. lattice does not respect the translational symmetry from the point of view of these orientations.

In the low-temperature phase III, the molecule occupies only one equilibrium position in one site. The uniaxial rotation motion observed by NMR (Amoureux, 1980) must then be viewed as a threefold rotation.

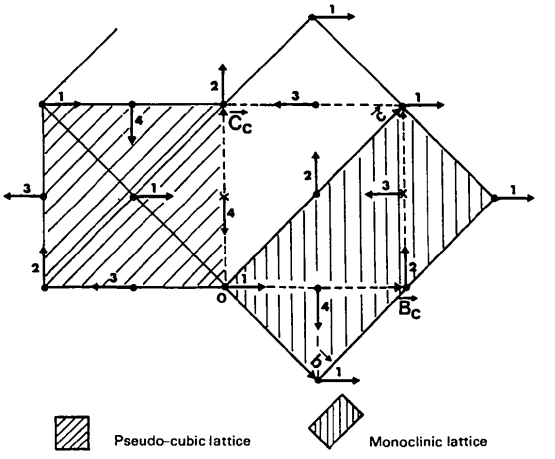

(*a*)

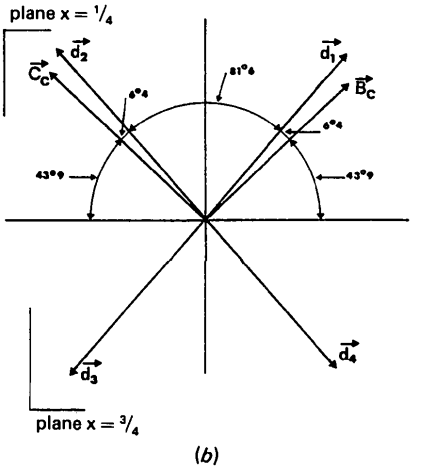

(*b*)

Fig. 8. (*a*) Relation between the pseudo-cubic and monoclinic lattices with schematic representation of molecular orientations. (*b*) Orientations of the dipolar axes $\mathbf{d}_i$ (C_3 molecular axes), in the ($\mathbf{B}_c$, $\mathbf{C}_c$) pseudo-cubic planes.

The transition to the plastic phase is accompanied by the appearance of tumbling movements which lead to six different equiprobable orientations in one site for a molecule. That transition is coherent with the creation of six domains. Zielinski & Foulon (1987) showed that the transition can be interpreted according to Landau theory in terms of the order parameter. The transition is induced by the interaction between displacive and orientational modes belonging to the (k_4, τ^3) irreducible representation.

References

AMOUREUX, J. P. (1980). Thesis, University of Lille I, France.

AMOUREUX, J. P. & BEE, M. (1979). *Acta Cryst.* B**35**, 2957–2962.

AMOUREUX, J. P., BEE, M. & SAUVAJOL, J. L. (1982). *Mol. Phys.* **45**, 709–719.

ANDRÉ, D., FOURME, R. & RENAUD, M. (1971). *Acta Cryst.* B**27**, 2371–2380.

BEE, M. & AMOUREUX, J. P. (1983). *Mol. Phys.* **48**(1), 68–79.

CHANG, S. S. & WESTRUM, F. F. (1960). *J. Phys. Chem.* **64**, 1547.

CLARK, T., MCKNOX, O., MACKLE, H. & MCKERVEY, M. A. (1977). *J. Chem. Soc. Faraday Trans.* **73**, 1224–1231.

FOULON, M. (1987). Thesis, University of Lille I, France.

FOULON, M., AMOUREUX, J. P., SAUVAJOL, J. L., CAVROT, J. P. & MULLER, M. (1984). *J. Phys. C*, **17**, 4213–4229.

FOULON, M., LEFEBVRE, J., AMOUREUX, J. P., MULLER, M. & MAGNIER, D. (1985). *J. Phys. (Paris)*, **46**, 919–926.

HAMILTON, W. C. (1965). *Acta Cryst.* **18**, 502–510.

HAMILTON, W. C. & ABRAHAMS, S. C. (1972). *Acta Cryst.* A**28**, 215–218.

HOVMOLLER, S., SMITH, G. & KENNARD, C. H. L. (1978). *Acta Cryst.* B**34**, 3016–3021.

PRESS, W. & HÜLLER, A. (1973). *Acta Cryst.* A**29**, 252–256.

SCHOMAKER, V. & TRUEBLOOD, K. N. (1968). *Acta Cryst.* B**24**, 63–76.

SEYMOUR, R. S. & PRYOR, A. W. (1970). *Acta Cryst.* B**26**, 1487–1491.

SHELDRICK, G. M. (1976). *SHELX*76. Program for crystal structure determination. Univ. of Cambridge, England.

SHIELDS, K. G. & KENNARD, C. H. L. (1983). *J. Chem. Soc. Perkin Trans.* 2, pp. 1374–1376.

URSU, I., GROSESCU, R., LUPU, M. & LAZARESCU, M. (1983). *Rev. Roum. Phys.* **28**(9), 789–814.

VIRLET, J., QUIROGA, L., BOUCHER, B., AMOUREUX, J. P. & CASTELAIN, M. (1983). *Mol. Phys.* **48**(6), 1289–1303.

ZIELINSKI, P. & FOULON, M. (1987). *Dynamics of Molecular Crystals: 41st International Meeting*, edited by J. LACOMBE. Amsterdam: Elsevier.

Acta Cryst. (1989). B**45**, 411–416

Crystal Structure and Direction of the Polar Axis of (−)-(1*S*)-Pinonic Acid β-Oxime

BY K. PADMANABHAN, I. C. PAUL* AND D. Y. CURTIN*

Department of Chemistry, University of Illinois, Urbana, IL 61801, *USA*

(*Received* 4 *November* 1988; *accepted* 21 *March* 1989)

Abstract

(−)-(1*S*)-*cis*-3-(Hydroxyiminoethyl)-2,2-dimethylcyclobutylacetic acid, $C_{10}H_{17}NO_3$, $M_r = 199{\cdot}25$, monoclinic, $P2_1$, $a = 14{\cdot}632\ (8)$, $b = 12{\cdot}193\ (3)$, $c = 7{\cdot}103\ (2)$ Å, $\beta = 112{\cdot}54\ (3)°$, $V = 1170{\cdot}5\ (8)$ Å^3, $Z = 4$ (two independent molecules in the asymmetric unit), $D_x = 1{\cdot}130$ g cm^{-3}, Mo $K\alpha$, $\lambda = 0{\cdot}71073$ Å, $\mu = 0{\cdot}69$ cm^{-1}, $F(000) = 432$, $T = 295$ K, $R = 0{\cdot}047$ for 1156 observed reflections [$I > 2{\cdot}5\sigma(I)$] and 257 parameters. Calculation suggests that the polarization of molecules of the (−)-enantiomer, oriented as in the crystal, is such that the positive end of the crystal's electric dipole is toward the + end of the *b* axis; conversely, for the (+)-enantiomer the polarization is in the opposite sense with the electrically positive end of the crystal dipole toward −*b*. This electrical polarization, due to the molecular orientation found from the crystal structure determination, is in the same direction as the polarization of the crystal produced by heating (the pyroelectric effect) as determined by the Kundt–Bürker powder test. Thus, as has been found in previous examples, the orientation along the polar axis of the electric dipole induced by heating is the same as the orientation of the polarization of the crystal deduced from the X-ray structure.

Introduction

The determination of the crystal structure of chiral (−)-(1*S*)-*cis*-3-(hydroxyiminoethyl)-2,2-dimethylcyclobutylacetic acid [(−)-pinonic acid β-oxime, (−)-(1)]

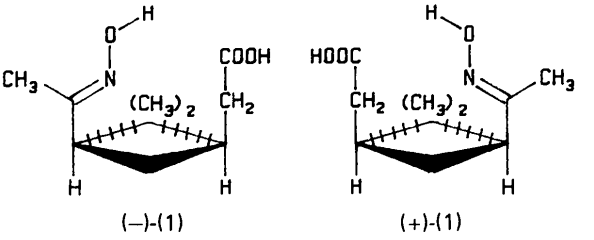

was carried out as part of an investigation of the utility of the Kundt–Bürker pyroelectric test for assigning the

* Authors to whom correspondence should be addressed.

0108-7681/89/040411-06$03.00